J Solid State Electrochem (2008) 12:1435–1443
DOI 10.1007/s10008-007-0485-z

ORIGINAL PAPER

Electrodeposition of Zn–TiO_2 nanocomposite films—effect of bath composition

J. Fustes · A. Gomes · M. I. da Silva Pereira

Received: 31 July 2007 / Revised: 14 November 2007 / Accepted: 28 November 2007 / Published online: 9 January 2008

Abstract Zn–TiO_2 nanocomposite films were prepared by pulsed electrodeposition from acidic zinc sulphate solutions on a Ti support. The influence on the composite structural and morphological characteristics of Zn^{2+} and TiO_2 concentrations in the deposition bath has been investigated. The characterisation of the samples was made by X-ray diffraction and scanning electron microscopy coupled with energy-dispersive X-ray spectroscopy (SEM/EDS). For all the obtained coatings, the anatase and rutile phases' most intense diffraction lines were observed between 24° and 28° 2θ, confirming the formation of the Zn–TiO_2 nanocomposite. X-ray diffraction data show that the presence of the TiO_2 nanoparticles plays a remarkable influence on the preferred orientation of the metal matrix. For the more diluted solution, a dependence between the metallic matrix grain size and the concentration of TiO_2 in bath is observed. The grain size decreases with the increasing on the nanoparticle amounts. The SEM results for Zn and Zn–TiO_2 deposits indicate that the nanoparticles have a strong influence on the deposit surface morphology, which is caused by the changes on the deposition mechanism.

Keywords TiO_2 · Metal matrix · Nanocomposite materials · Electrodeposition · Preferred orientation

J. Fustes · A. Gomes (✉) · M. I. da Silva Pereira
C.C.M.M., Departamento de Química e Bioquímica da Faculdade de Ciências da Universidade de Lisboa,
Campo Grande,
1749-016 Lisbon, Portugal
e-mail: abmg@fc.ul.pt

Introduction

Electrolytic co-deposition is widely used for preparing metal matrix composites because of its low cost and versatility [1]. By electrolysis of plating solutions, in which micron or sub-micron size particles are suspended, it is possible to obtain novel materials with improved and/or combined properties, which make them interesting for different applications such as electrocatalysis and photo-electrocatalysis.

The electrolytic co-deposition of inert particles and metals is a very complex process. Although several experimental and theoretical studies on particle co-deposition mechanism have been published, the process is not yet well understood. Several theories have been proposed, including the transport of particles owing to electrophoresis, mechanical entrapment, adsorption and convective-diffusion [2]. The progressive development of the electrodeposit texture and roughening takes place during the particles' inclusion into the metallic deposit.

Composites containing occluded TiO_2 nanoparticles are interesting materials because of the TiO_2 semiconducting properties, with applications as photocatalyst and photo-electrocalyst, particularly on the treatment of polluted water [3]. In the last years, a lot of work has been performed on the TiO_2 co-deposition process, with the metallic component being Ni, Cu, Ag and Zn [4–6].

The nanocomposite characteristics are influenced by the deposition parameters, namely current profile, bath composition, pH, particles concentration and temperature [7].

Pulsed direct current is an alternative technique to direct current for the preparation of composite films, which allows the tailoring of the deposit properties. The application of a pulsed current enables the incorporation of higher concen-

trations of particles in addition to a wider range of deposit compositions [2].

In a previous work, we have used successfully this technique on the preparation of Zn–TiO_2 nanocomposite films on a Fe substrate. The influence of the pH and presence of surfactants on the deposit properties have been studied. It has been found that the zinc matrix crystal orientation changes with the pH value of the electroplating bath. Moreover, the presence of the surfactant led to a decrease on the metallic grain size [8].

The goal of the present work is to investigate the influence of Zn^{2+} and TiO_2 concentrations in the deposition bath on the structural and morphological characteristics of the as-deposited nanocomposites, which are crucial for their photocatalytic performance [9]. It is expected that a lower concentration of electroactive species favours the formation of a electrodeposit with well-dispersed and less-agglomerated nanoparticles [2].

Experimental

The electroplating bath was prepared with $ZnSO_4 \cdot 7H_2O$ (Riedel-deHaën p.a.), $MgSO_4$ (Merck p.a.), H_3BO_3 (M&B p.a.) and TiO_2 (Degussa P25, particle size approx. 25 nm, with chemical composition of 80% anatase and 20% rutile). Table 1 presents the composition of the deposition baths. The used concentrations of $MgSO_4$ and H_3BO_3 with respect to $ZnSO_4$ were selected on the basis of a constant ratio between them of ≈2. The concentrations of TiO_2 in the bath were 1.0, 1.6, 10 and 16 g/l. The bath pH was adjusted to 4 by adding a diluted solution of H_2SO_4. The solutions were made daily without further purification followed by deaeration with nitrogen before and during the electrodeposition.

A glass cell with two compartments was used, with a Zn plate as counter electrode and a commercial Ag/AgCl as reference. The working electrode was a Ti disc (Goodfellow) with a 10-mm diameter. The Ti disc was etched with HF 40%, polished with 0.05-μm silica powder (Buehler) and ultrasonically cleaned for 10 min in pure water.

The Zn–TiO_2 nanocomposite films were prepared by pulse electrodeposition, using a galvanostatic cathodic square wave with a pulse peak current of −255 mA cm^{-2}

Table 1 Bath composition

Bath	Concentration/mol dm^{-3}		
	$ZnSO_4$	$MgSO_4$	H_3BO_3
1	0.5	1.0	0.25
2	0.3	0.6	0.15
3	0.1	0.2	0.05

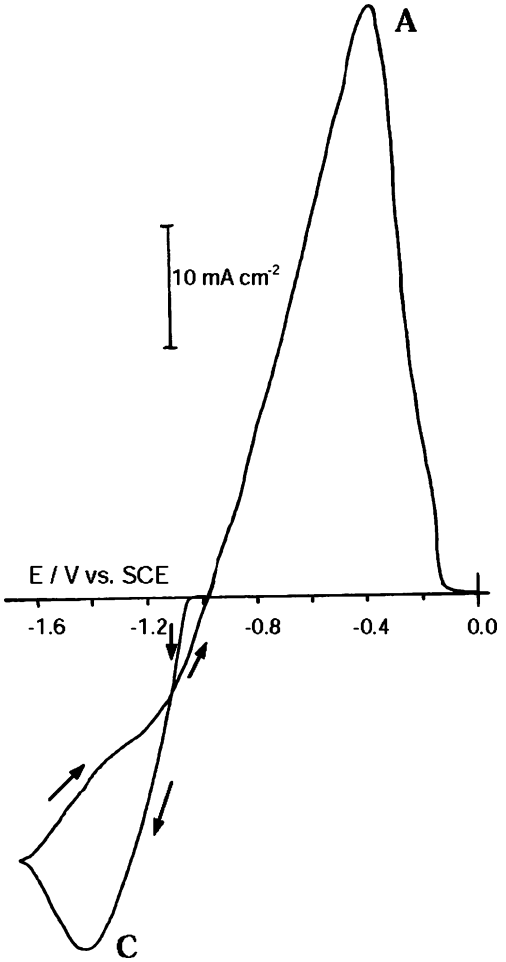

Fig. 1 Cyclic voltammogram obtained for titanium electrode from bath 1. Scanning rate 10 mV s^{-1}

and the current on-time and off-time of 4 and 40 ms, respectively. The deposition was performed under magnetic stirring (400 rpm) at room temperature for 1 h. When finished, the electrode was removed from the cell, rinsed with deionised water (18 MΩ cm) and dried under a nitrogen atmosphere at room temperature for 5–10 min.

The mass of the electrodeposits was evaluated by weighing the samples before and after the electrodeposition. The theoretic mass value was calculated using Faraday's law.

Voltammetric experiments were carried in a three-electrode glass cell with a titanium disc as working electrode, a platinum spiral as counter electrode and a commercial Ag/AgCl as reference electrode. All potentials are reported with respect to this reference.

The electrochemical measurements were carried out using an EG&G Princeton Applied Research potentiostat/galvanostat, Model PAR 263, connected to a Philips PM 8271 recorder.

X-ray diffraction (XRD) analysis of the electrodeposits was carried out using a Philips X-ray diffractometer (model

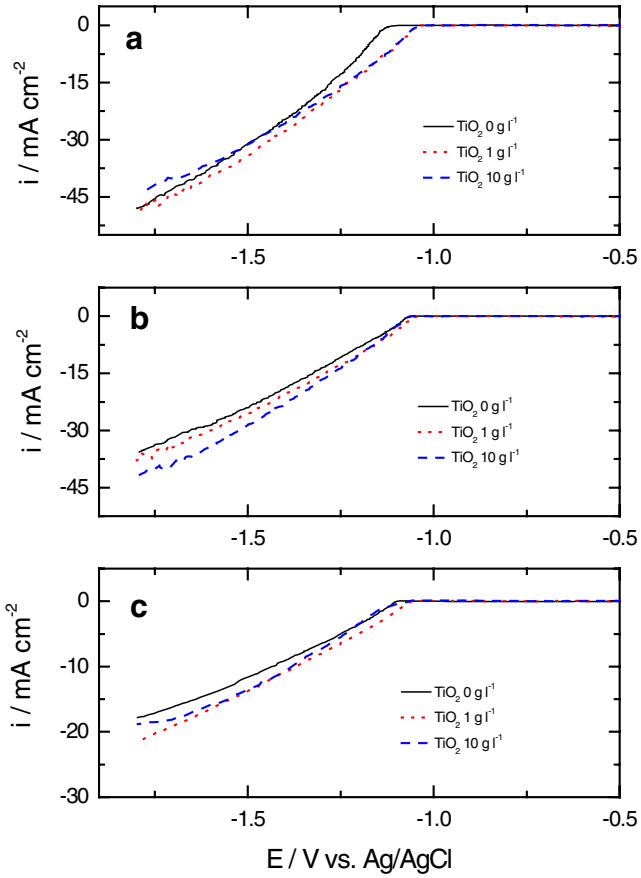

Fig. 2 Current potential curves for a titanium electrode in baths **a** 1, **b** 2 and **c** 3. Scanning rate 2 mV s^{-1}

PW 1710) with Cu Kα radiation (λ=0.15604 nm), working at 30 mA and 40 kV. The diffractograms were obtained in the 2θ range of 20° to 80°, using a 0.02° step and acquisition time of 2 s/step. Measurements with acquisition time of 10 s/step were made in the 2θ range of 22 to 30°.

The preferred orientation of the zinc electrodeposits was estimated from the X-ray data according to the methodology developed by Bérubé and L'Espérance [10], where the texture coefficient (T_c) is calculated by using the equation above:

$$T_c = \left(I_{(hk.l)} \Big/ \sum I_{(hk.l)}\right) \times \left(\sum I_{p(hk.l)} \Big/ I_{p(hk.l)}\right) \quad (1)$$

where $I_{(hk.l)}$ is the diffraction line intensity of the (hk.l) reflection of zinc electrodeposits, $\Sigma I_{(hk.l)}$ is the sum of the intensities of all the diffraction lines monitored. The index p refers to the reference zinc powder sample. A value of T_c greater than 1 indicates a preferred orientation of the (hk.l) reflection compared with the random distribution of the grains in the reference zinc powder [10].

The grain size of the zinc crystallites was obtained by using the Scherrer equation

$$D = (K\lambda)/(B\cos\theta) \quad (2)$$

where D is the diameter of the crystal particle, K the shape factor (the typical value is 0.9), λ the wavelength of the incident beam, B the broadening of the diffraction line measured in radians at half of its maximum intensity and θ the Bragg angle [11].

The films' morphology and elemental composition were investigated by scanning electron microscopy (SEM)/energy-dispersive spectroscopy (EDS). Scanning electron microscopy coupled with EDS analysis was performed with a JEOL (JSM-6301F) microscope with an electron beam voltage of 15 kV.

Results and discussion

Voltammetric studies

A typical cyclic voltammogram of titanium recorded in 0.5 mol dm^{-3} Zn^{2+} solution between 0.0 and −1.7 V vs. Ag/AgCl at 10 mV s^{-1} is shown in Fig. 1. The voltammogram presents a sharp cathodic peak C (E_{pc}=−1.4 V) because of the reduction of the metallic ions and the corresponding anodic stripping peak A (E_{pa}=−0.4 V). After this peak, the anodic current goes to zero, indicating that the majority of the zinc deposit has been removed. In the cathodic region, the hydrogen evolution also occurs as it is detected by direct observation.

Upon the sweep reversal, two current crossovers appear because of the formation of stable growth centres at the substrate surface [12].

For the systems containing 0.3 and 0.1 mol dm^{-3} Zn^{2+} ions, the cathodic peak is slightly displaced to the right side, and the peak current density decreases.

Table 2 Electroplating conditions and average mass deposited

Electroplating conditions		Average mass of deposit/ mg cm^{-2}
Bath	TiO_2/g l^{-1}	
1	16	29.2
	10	29.4
	1.6	28.2
	1.0	28.4
	0.0	28.3
2	16	31.7
	10	28.3
	1.6	27.5
	1.0	29.2
	0.0	28.0
3	16	19.5
	10	13.4
	1.6	11.6
	1.0	16.3
	0.0	26.2

The influence of the potential scan rate (ν) on the Zn deposition has been investigated. The data reveals that an increase in sweep rate shifts the peak potential to more negative values and increases the peak current. The relation between the cathodic peak current density and the square root of scan rate ($\nu^{1/2}$) is linear, but the lines do not pass through the origin. The linearity is predictable for a reduction processes that occurs under mass transfer control. However, the positive intercept indicates that an additional process other than diffusion occurs [13].

The estimated charge density of the anodic peak is 2,809, 1,641 and 569 mC cm^{-2} for the systems containing 0.5, 0.3 and 0.1 mol dm^{-3} Zn^{2+} ions, respectively. These values show, as expected, that the amount of deposited Zn is proportional to the concentration of metallic ions in the bath.

Figure 2 shows the linear voltammograms obtained for the different baths in the absence and presence of different amounts of TiO_2 under stirring.

As expected, in the absence of semiconductor particles, the cathodic current decreases when the Zn^{2+} ions' concentration is reduced. This fact points out that the deposition rate is lower when the metallic ions' concentration decreases.

In the presence of the semiconductor particles, a slight increase on the current density is observed, indicating that the TiO_2 particles promote the zinc deposition. It can be assumed that the increase on the current density is due to the adsorption of the titania particles on the cathode surface which would lead to an enhanced surface area [14].

Electrodeposition

The electrodeposit amount obtained from the different plating solutions, which is used in this work, is presented in Table 2. As it can be seen, the average mass of the deposits obtained in absence of titania particles is very

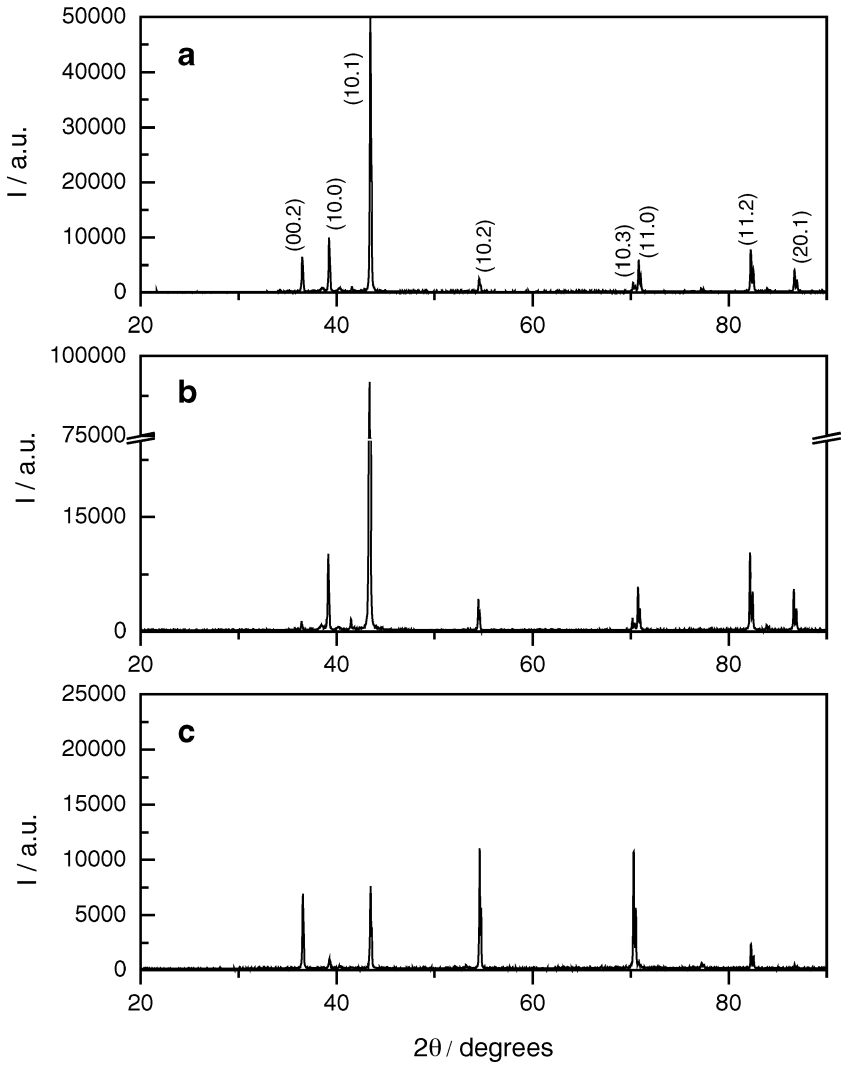

Fig. 3 XRD patterns of Zn films prepared from different baths **a** 1, **b** 2 and **c** 3

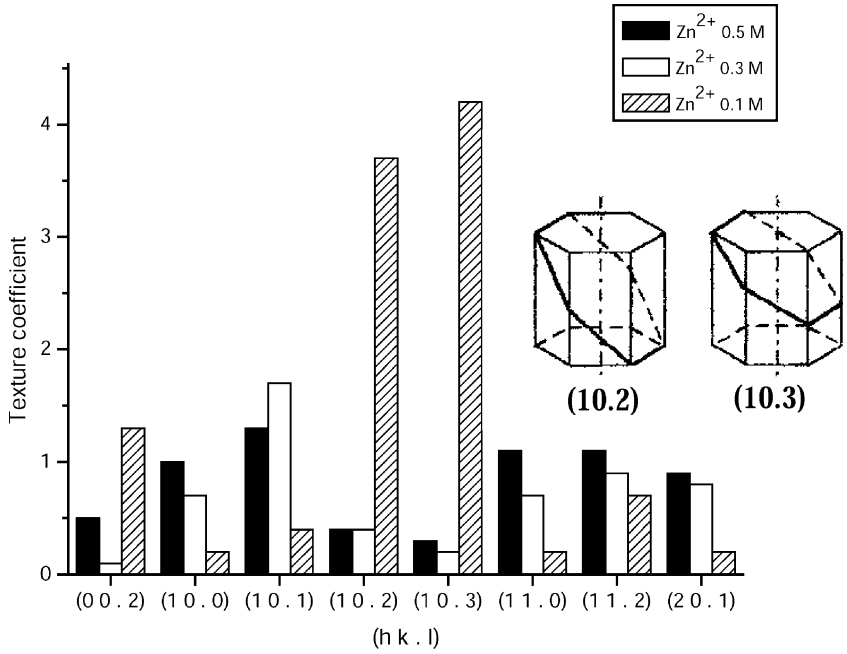

Fig. 4 Preferential orientation for the Zn films prepared from different baths

similar to the theoretic value, 28 mg cm^{-2}, for solutions 1 and 2 and, lower for solution 3. Assuming that the deposit is uniformly distributed on the substrate surface, the thickness of the metallic electrodeposit has been estimated. The obtained values vary between 39 and 36 μm. The lowest value is explained by a strong hydrogen production that competes with the metal deposition. Moreover, the hydrogen gas bubbles adhere to the cathode surface, preventing the deposition process.

For the nanocomposite films, the data show that the deposit mass average increases slightly with the amount of TiO_2 in the bath for solutions 1 and 2, while for solution 3, the deposit presents the lowest mass average value. As explained before, this fact is a consequence of the strong hydrogen evolution.

Structural studies

The XRD patterns of the zinc films, prepared from the three different Zn^{2+} solutions, are presented in Fig. 3. Considering that the estimated thickness for all the films is similar, the diffractograms were compared. The analysis of the diffractograms indicates that the composition of the Zn deposition bath has a strong influence on the orientation of the deposits. The majority of the diffraction lines can be ascribed to the Zn hexagonal structure [15] as usually detected for these deposits [16, 17]. The calculated texture coefficients are plotted in Fig. 4, where the inset shows, in the scheme, some crystallographic orientations in zinc hcp crystals, namely the (10.2) and (10.3) planes. It can be seen that for the samples prepared from 0.5 and 0.3 mol dm^{-3} Zn^{2+} solutions, the majority of the zinc crystallites are oriented parallel to the (10.1) plane, while for those prepared from the 0.1 mol dm^{-3} Zn^{2+} solution, the preferential crystallographic orientation of the zinc deposit is (10.3). As it has been referred previously, in this case, a strong hydrogen co-evolution is observed, which may be responsible for the development of a different

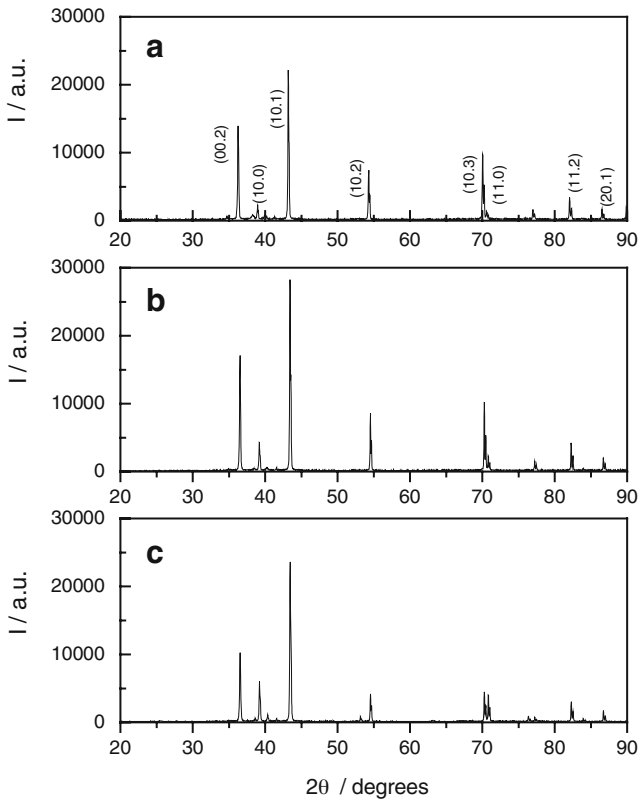

Fig. 5 XRD patterns of Zn–TiO_2 films, prepared from different baths **a** 1, **b** 2 and **c** 3 with 16 g/l TiO_2. Only Zn peaks were identified

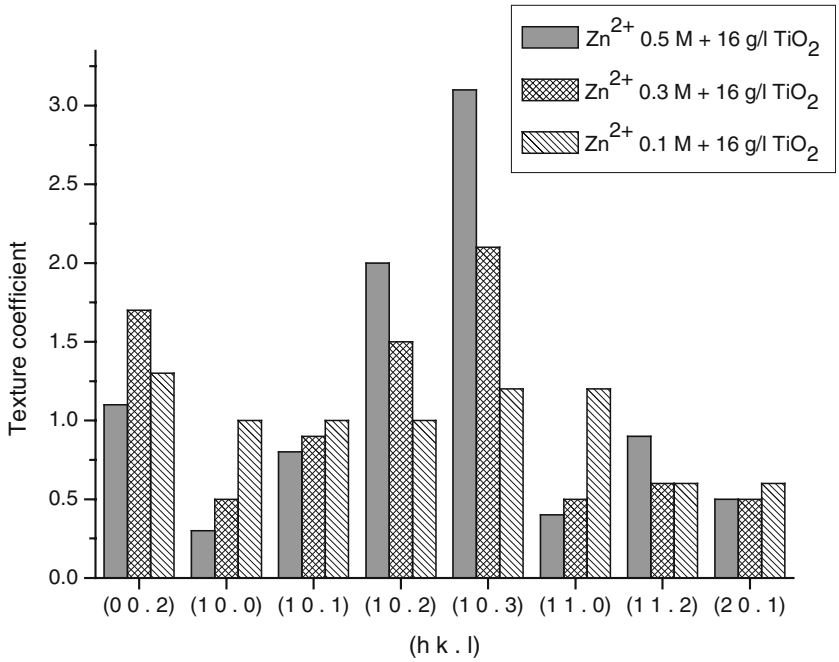

Fig. 6 Preferential orientation for the Zn films prepared from different baths containing 16 g/l TiO_2

texture. It is referred in the literature that pyramidal high index (10.*X*) (*X*=3, 4, 5) orientation is dominant at relatively high pH (>4.5) [18]. Additionally, a lower Zn^{2+} concentration may promote the hydrogen adsorption on the Zn active sites and selectively influences the growth rates of the various zinc crystal planes.

The patterns for the Zn–TiO_2 composite films electrodeposited from the three different Zn^{2+} solutions are shown in Fig. 5. X-ray diffraction data is presented only for the deposits obtained from the deposition bath containing 16 g/l TiO_2. For the other samples, the results are similar. The analysis of the diffractograms shows that the majority of the diffraction lines can be ascribed to the Zn hexagonal structure similarly to the films prepared in the absence of TiO_2 nanoparticles [15]. However, in the presence of the TiO_2 particles, a modification on the crystallographic orientation of the zinc matrix crystallites occurs comparatively with the samples prepared in the absence of TiO_2 nanoparticles, as Fig. 6 indicates. More precisely, for the samples prepared from 0.5 and 0.3 mol dm^{-3} Zn^{2+} solutions, the preferred crystallographic orientation changes from (10.1) to (10.3) plane, while for those prepared from the 0.1 mol dm^{-3} Zn^{2+} solution, the zinc matrix crystallizes preferentially in (00.2), (10.3) and (11.0) textures. These results indicate that the presence of the TiO_2 nanoparticles plays a remarkable influence on the preferred orientation of the metal matrix as a consequence of changes

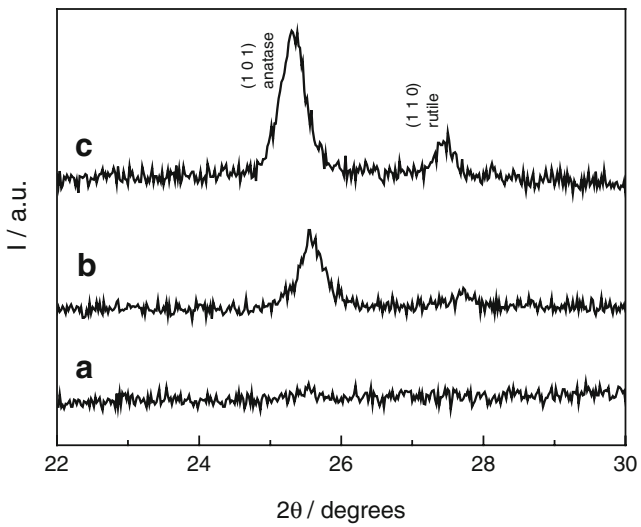

Fig. 7 XRD patterns obtained between 22° and 30° 2θ for Zn–TiO_2 films prepared from the different baths: **a** 1, **b** 2 and **c** 3 containing 16 g/l TiO_2

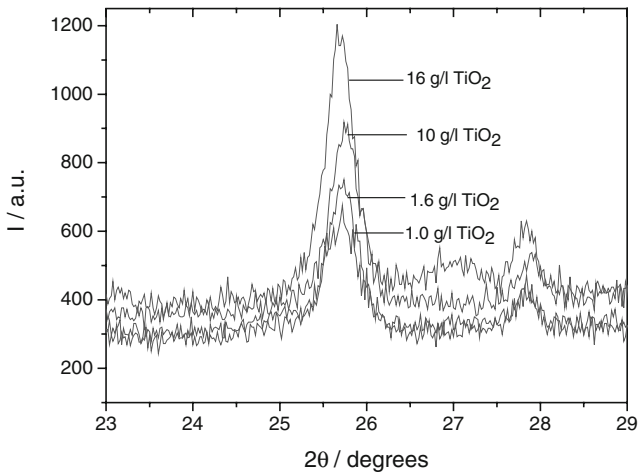

Fig. 8 XRD patterns of Zn–TiO_2 films prepared from bath 1 with different concentrations of TiO_2

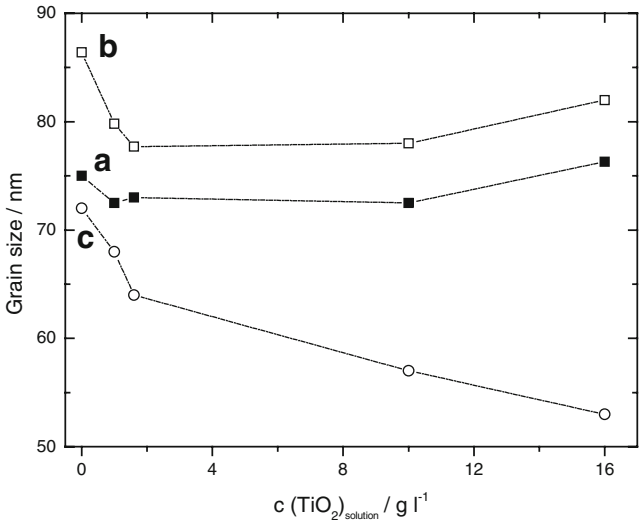

Fig. 9 Metallic matrix grain size variation with Zn^{2+} and TiO_2 concentrations in bath: **a** 1, **b** 2 and **c** 3

on the metal deposition mechanism. This result is in accordance with that stated in the literature, that the particles embedded in the coatings can affect the preferred orientation of the metallic matrix [19, 20].

The variation on the titania contents in the nanocomposite coatings was also estimated by XRD analysis. For all the obtained electrodeposits prepared in the presence of TiO_2, the (1 0 1) and (1 1 0) diffraction lines for anatase and rutile phases, respectively, were observed between 24° and 28° 2θ [21]. This result confirms the formation of the Zn–TiO_2 nanocomposite [8]. As Fig. 7 shows, when the concentration of the Zn^{2+} ions in the electrolyte decreases, the intensity of the titania diffraction lines increases, indicating that the content of the titania particles increases in the nanocomposite coatings. This fact should be associated to a modification on the zinc deposition, which improves the incorporation of the inert particles. Additionally, with the decreasing solution ionic strength, the thickness of the diffuse double layer around the particles increases, which promotes the dispersion of the nanoparticles in the electrolyte. The smaller particle agglomerates have a higher probability to be embedded in the metal matrix than larger ones.

Figure 8 presents diffractograms taken from the deposits prepared from 0.1 mol dm^{-3} Zn^{2+} solution with different concentrations of TiO_2 particles. The data suggest that the peaks' intensity increases when the TiO_2 concentration goes up in the solution, indicating an enhancement in the co-deposition, which is expected from that referred in the literature [22].

Although the XRD peaks are narrow, the grain size of the metallic matrix has been estimated from the width of the zinc (1 0. 1) diffraction line. The obtained information gives an apparent magnitude that is quite useful for comparative studies. Figure 9 shows, as expected, that the Zn ions' concentration influences the crystal growth of the metallic matrix. It is interesting to note that the higher grain size values were obtained for the solution containing 0.3 mol dm^{-3} zinc ions. An explanation for this was not yet established.

In what concerns the dependence on the amount of TiO_2 present in solution, different tendencies are observed following the zinc ions' concentration in the solution. For the more concentrated solutions in metallic ions, the grain size of the metallic matrix is practically independent on the TiO_2 concentration, although a slight increase is observed on the grain size for the matrixes prepared in the presence of the highest concentration of TiO_2. On the contrary, for the more diluted solution, dependence between the metallic matrix grain size and the concentration of TiO_2 in bath is observed: The grain size decreases with the increasing on the nanoparticles amount. This fact can be mainly related to modifications on the nucleation and growth of the zinc crystallites because of the zinc ions' concentration and presence of the semiconductor particles. For the more diluted solution, the hydrogen co-evolution and the presence of particles should have a detrimental effect on crystal growth, leading to smaller grain size of the zinc matrix. Similar results were obtained for the deposition of nickel in the presence of silicon carbide nanoparticles [23].

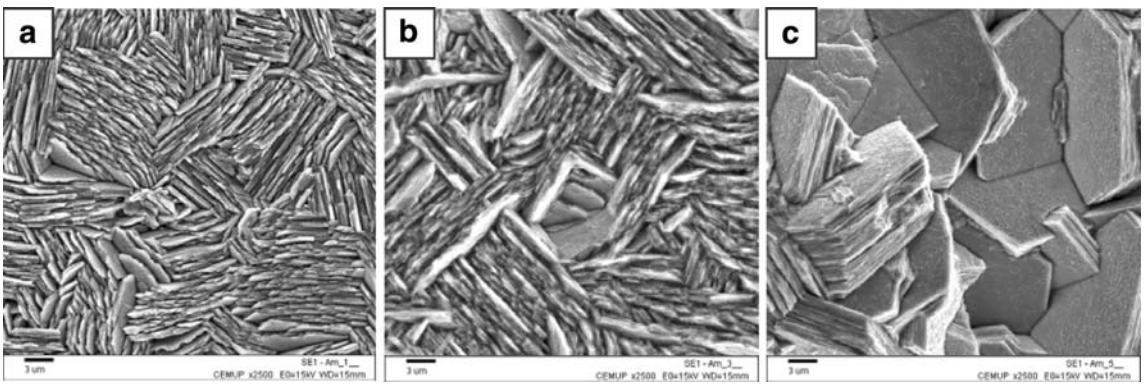

Fig. 10 SEM micrographs of the surface of Zn films prepared from baths **a** 1, **b** 2 and **c** 3

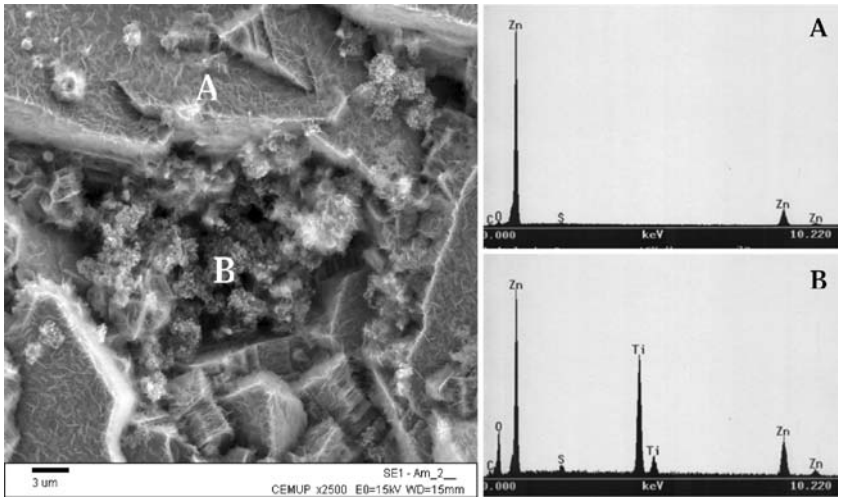

Fig. 11 SEM micrograph and EDS spectra for different points on the surface of a Zn–TiO_2 composite film prepared from bath 1 with 16 g/l TiO_2

Morphological studies

Figure 10a–c shows the morphology of zinc electrodeposits obtained in the absence of TiO_2 nanoparticles from 0.5, 0.3 and 0.1 mol dm^{-3} Zn^{2+} solutions, respectively. As it can be seen, the morphology changes in function of the Zn^{2+} ions' concentration. Figure 10a and b shows a "ridge morphology" where the grains are aligned vertically in different directions. For the deposits obtained from the Zn^{2+} solution with the lowest concentration, Fig. 10c, the zinc crystallites present hexagonal-shape oriented nearly parallel to the substrate, in accordance with the structural studies.

Figure 11 presents a SEM image and the corresponding EDS spectra for an electrodeposit obtained from the 0.5 mol dm^{-3} Zn^{2+} system that confirms the presence of the TiO_2 particles in the electrodeposited composite. Energy-dispersive spectroscopy analysis performed for all electrodeposited composite films allowed the identification of areas where the presence of Ti in addition to an increase of the oxygen content occur, indicative of the presence of TiO_2 particles.

Figure 12 contains SEM images of the Zn–TiO_2 nanocomposite films prepared from the three metallic concentration systems with the highest TiO_2 concentration. These data reveal a morphology that is quite distinct from the Zn deposits. Indeed, the metallic grains present a different shape from that observed in the metallic coatings, which was expected from the structural studies. The SEM results coupled with the XRD data for Zn and Zn–TiO_2 deposits indicate that the particles have a strong influence on the deposit surface morphology, which is caused by the changes on the deposition mechanism.

Conclusions

Zn–TiO_2 nanocomposite coatings on titanium discs were successfully prepared by pulsed direct current using a zinc plating bath with homogeneously dispersed TiO_2 nanoparticles. For all the obtained coatings, the (1 0 1) and (1 1 0) diffraction lines for anatase and rutile phases, respectively, were observed between 24° and 28° 2θ, confirming the formation of the Zn–TiO_2 composite.

It was found that the Zn^{2+} ions' concentration and the presence of the TiO_2 nanoparticles play a remarkable influence on the preferred orientation of the metal matrix. For the nanocomposites prepared from 0.5 and 0.3 mol dm^{-3}

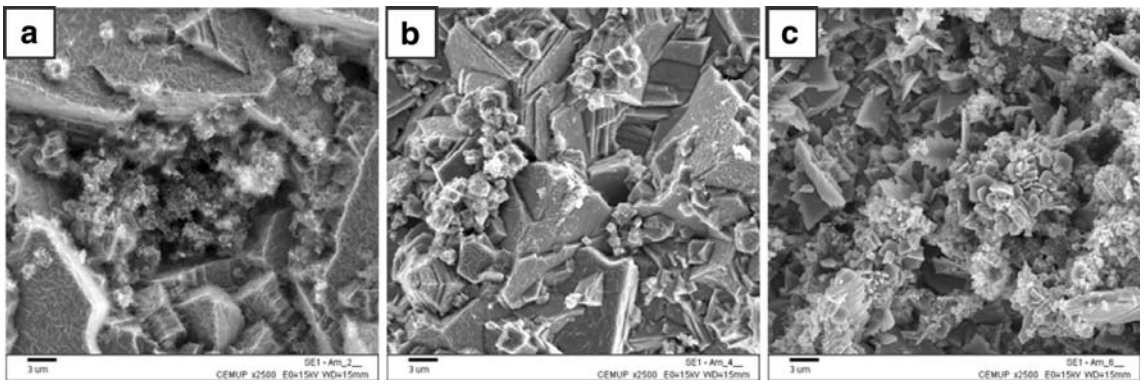

Fig. 12 SEM micrographs of the surface of Zn–TiO_2 films prepared from baths: **a**) 1, **b**) 2 and **c**) 3 with 16 g/l TiO_2

Zn^{2+} solutions, the preferred crystallographic orientation changes from (10.1) to (10.3) plane, while for those prepared from the 0.1 mol dm^{-3} Zn^{2+} solution, the zinc matrix crystallizes preferentially in (00.2), (10.3) and (11.0) textures.

For the more concentrated solutions in metallic ions, the grain size of the metallic matrix is practically independent on the TiO_2 concentration, although a slight increase is observed on the grain size for the matrixes prepared in the presence of the highest concentration of TiO_2. On the contrary, for the more diluted solution, dependence between the metallic matrix grain size and the concentration of TiO_2 in bath is observed. The grain size decreases with the increasing on the nanoparticles amount.

The SEM results for Zn and Zn–TiO_2 deposits indicate that the nanoparticles have a strong influence on the deposit surface morphology, which is caused by the changes on the deposition mechanism.

Acknowledgements The authors acknowledge the financial support and A. Gomes acknowledges the SFRH/BPD/11605/2002 grant from the Fundação para a Ciência e Tecnologia, Portugal.

References

1. Bard AJ, Stratmann M (2002) Semiconductor electrodes and photoelectrochemistry. In: Licht S (ed) Encyclopedia of electrochemistry, vol 6. Wiley-VCH, Weinheim, p 44
2. Low CTJ, Wills RGA, Walsh FC (2006) Surf Coat Technol 201:371
3. Fujishima A, Rao TN, Tryk DA (2000) J Photochem Photobiol C: Photochem Rev 1:1
4. Ito S, Deguchi T, Imai K, Iwasaki M, Tada H (1999) Electrochem Solid-State Lett 2:440
5. De Tacconi NR, Boyles AA, Rajeshwar K (2000) Langmuir 16:5665
6. Deguchi T, Imai K, Matsui H, Iwasaki M, Tada H, Ito S (2001) J Mater Sci 36:4723
7. Zhou M, de Tacconi NR, Rajeshwar K (1997) J Electroanal Chem 421:111
8. Gomes A, da Silva Pereira MI, Mendonça MH, Costa FM (2005) J Solid State Electrochem 9:190
9. Pozzo RL, Baltanás MA, Cassano AE (1997) Cat Today 39:219
10. Bérubé LPh, L'Espérance G (1989) J Electrochem Soc 136:2314
11. Cullity BD (1978) Elements of X-ray diffraction, 2nd edn. Addison-Wesley, p 284
12. Fletcher S, Halliday CS, Gates D, Westcott M, Lwin T, Nelson G (1983) J Electroanal Chem 159:267
13. Trejo G, Ortega R, Meas Y, Ozil VP, Chainet E, Nguyen B (1998) J Electrochem Soc 145:4090
14. Aslanidis D, Fransaer J, Celis JP (1997) J Electrochem Soc 144:2352
15. Power Diffraction File Alphabetical Index (1988) JCPDS-ICDD International Center for Diffraction Data (ed), Swarthmore, USA File 4-0831
16. Gomes A, da Silva Pereira MI (2006) Electrochim Acta 51:1342
17. Gomes A, da Silva Pereira MI (2006) Electrochim Acta 52:863
18. Vasilakopoulos D, Bouroushian M, Spyrellis N (2006) J Mater Sci 41:2869
19. Hou F, Wang W, Guo H (2006) Appl Surf Sci 252:3812
20. Benea L, Bonora PL, Borello A, Martelli S (2001) J Electrochem Soc 148:995
21. Power Diffraction File Alphabetical Index (1988) JCPDS-ICDD International Center for Diffraction Data (ed), Swarthmore USA File 21-1272 for anatase, File 21-1276 for rutile
22. Hovestad A, Heesen RJCHL, Janssen LJJ (1999) J Appl Electrochem 29:331
23. Benea L, Bonora PL, Borello A, Martelli S, Wenger F, Ponthiaux P, Galland J (2001) J Electrochem Soc 148:C461